

Highly accurate Coiflet wavelet-homotopy solution of Jeffery-Hamel problem at extreme parameters

Sohail Ahmed, Hang Xu,* An-Yang Wang, Qing-Bo Chen

State Key Lab of Ocean Engineering, School of Naval Architecture,
Ocean and Civil Engineering, Shanghai Jiao Tong University, Shanghai 200240, China

*To whom correspondence should be addressed: hangxu@sjtu.edu.cn.

The magnetised Jeffery-Hamel flow due to a point sink or source in convergent and divergent channels is studied. The simplified governing equation ruled by the Reynolds number, the Hartmann number and the divergent-convergent angle with appropriate boundary conditions are solved by the newly proposed Coiflet wavelet-homotopy method. Highly accurate solutions are obtained, whose accuracy is rigidly checked. As compared with the traditional homotopy analysis method, our proposed technique has higher computational efficiency and larger applicable range of physical parameters. Results show that our proposed technique is very convenient to handle strong nonlinear problems without special treatment. It is expected that this technique can be further applied to study complex nonlinear problems in science and engineering involving into extreme physical parameters. Besides, the influence of physically important quantities on the flow is discussed. It is found that wall stretching and shrinking exhibits totally different roles on the flow development. The enhanced Lorenz force affects the flow behaviours significantly for both convergent and divergent cases.

1 Introduction

Incompressible viscous flow driven in convergent and divergent channels has numerous applications in the fields of fluid mechanics and civil, mechanical, bio-mechanical and environmental engineering. The famous Jeffery-Hamel problem [1, 2] is usually used to describe such fluid motion, which was then extended by many researchers to different physical configurations such as radial flow between two inclined plane walls [3], flow in symmetrical channels with slightly curved walls [4], magnetohydrodynamic

flow between convergent or divergent channels [5]. Like most classical problems in fluid mechanics, the class of Jeffery-Hamel problems does not admit analytical solutions. As a result, analytical and numerical approaches are common tools to give their solutions. In literature, many techniques including the spectral homotopy analysis method [6], the optimal homotopy asymptotic method [7], the Adomian decomposition method [8,9] and its modification [10], the perturbation method [11], the homotopy analysis method [12] and its insequential transformation [13,14], the predictor homotopy analysis method [15], the finite volume method [16] and the collocation method [17], have been suggested to attack such kind of convergent or divergent channel flow problems.

Among those computational techniques, the homotopy analysis method [18,19] was regarded as a very accurate and efficient approach for handling nonlinear problems with strong nonlinearity. This is due to that it is not dependent upon small or large physical parameters, has freedom to express the solution based on its behaviours, and can adjust convergent rate via a convergence-control parameter. Though having all above mentioned advantages, in our knowledge there is still a room to improve on this technique. Several obvious weaknesses of the homotopy analysis method are held. Firstly, it is very time-consuming for complicated nonlinear problems. Secondly, its convergent rate is rather slow when extreme large parameters are involved. Thirdly, it has limited solution expression forms. Yang and Liao [20,21] made efforts to overcome these issues by introducing the Coiflet wavelet functions [22–24] into the homotopy analysis method as the solution expressions. Their modified technique not only holds the advantages of strong nonlinear processing capability inherited by the homotopy analysis method and excellent local expression characteristics originated from the Coiflet wavelet, but also is very efficient and accurate for nonlinear equations with homogenous boundary conditions. Yu and Xu [25–27] established a generalized boundary modification approach based on the Coiflet wavelet which is suitable for both

ordinary and partial differential equations subjected to non-homogenous boundary conditions. Their idea was further adopted by Wang *et al.* [28] for a electrohydro-dynamic flow problem and Chen [29] for a channel flow problem, respectively.

In this paper, we shall further develop the Coiflet wavelet-homotopy method for handling nonlinear problems with extreme physical parameters. A complete set of solution solving process will be established based on both the homotopy analysis method and the Coiflet wavelet based on the famous MHD Jeffery-Hamel problem. Note that in most above mentioned studies, few researchers have considered such extreme case. This makes our work novel and unique. Highly accurate solution for a large range of physical parameters will be given, whose validity and efficiency will be strictly checked. The outline of this is organized as follows: In Section 2, mathematical modeling and formulations of the MHD Jeffery Hamel flow is presented. In Section 3, the fundamentals of Coiflet wavelet-homotopy method is given. In Section 4, results is verified and. In Section 5, the concluding remarks are drawn.

2 Mathematical Description

We consider a magnetohydrodynamic flow of an incompressible viscous conducting fluid due to either a source or a sink at the intersection of two stretchable or shrinkable nonparallel plane walls with an included angle 2β . The cases $\beta < 0$ and $\beta > 0$, respectively, denote the convergent and the divergent channels. The physical sketch is shown in Fig.1. The polar coordinates (r, θ, z) are employed, where r , θ and z denote the polar radius, polar angle and polar axis respectively. The flow is assumed to be laminar and symmetrical. The variable magnetic field \mathbf{B} is assumed to be perpendicular to the radial direction, whose distribution is $[B_0/r, 0, 0]$. The fluid parameters are assumed to remain unchanged

along z direction, as a result the flow is only dependent on r and θ . These assumptions indicate that the velocity field of the flow has the form $\mathbf{V} = [u_r, 0, 0]$, where $u_r = u(r, \theta)$ is a function of r and θ .

The governing equations for the flow are given, as suggested by Jeffery [1], as

$$\nabla \cdot \mathbf{V} = 0, \quad (1)$$

$$\rho \left[\frac{\partial \mathbf{V}}{\partial t} + (\mathbf{V} \cdot \nabla) \mathbf{V} \right] = -\nabla p + \mu \nabla^2 \mathbf{V} + \mathbf{F}, \quad (2)$$

where t denotes the time, \mathbf{V} , ρ , μ , p and \mathbf{F} are the velocity vector, the fluid density, the dynamic viscosity, the pressure and the Lorenz force (total electromagnetic force) respectively. Here the Laplacian operator is given by

$$\nabla^2 = \frac{\partial^2}{\partial r^2} + \frac{1}{r} \frac{\partial}{\partial r} + \frac{1}{r^2} \frac{\partial^2}{\partial \theta^2}. \quad (3)$$

Based on the Ohm's low, the Lorenz force is expressed by

$$\mathbf{F} = \mathbf{J} \times \mathbf{B}, \quad (4)$$

where \mathbf{J} is the electrical current density, defined by

$$\mathbf{J} = \sigma[\mathbf{E} + \mathbf{V} \times \mathbf{B}], \quad (5)$$

in which σ is the electrical conductivity, \mathbf{E} is the applied electrical field that is enforced to zero (refer to Xu *et al.* [31]).

On the other hand, the walls are assumed to be radially stretched or shrunk in accordance with

$$u = u_w = \frac{S_r}{r}, \quad (6)$$

where S_r is the stretching/shrinking rate. On the centreline, it holds

$$u_r = \frac{u_c}{r}, \quad \frac{\partial u_r}{\partial \theta} = 0, \quad (7)$$

where u_c is a reference velocity on the centreline.

For the steady case, the aforementioned equations are expanded, after a series of physical assumptions such as low magnetic Reynolds number and symmetrical flow, as

$$\frac{\partial}{\partial r}(ru_r) = 0, \quad (8)$$

$$u_r \frac{\partial u_r}{\partial r} + \frac{1}{\rho} \frac{\partial p}{\partial r} - \nu \left[\frac{\partial^2 u_r}{\partial r^2} + \frac{1}{r} \frac{\partial u_r}{\partial r} + \frac{1}{r^2} \frac{\partial^2 u_r}{\partial \theta^2} - \frac{u_r}{r^2} \right] + \frac{\sigma B_0^2}{\rho r^2} = 0, \quad (9)$$

$$\frac{1}{\rho r} \frac{\partial p}{\partial \theta} - \frac{2\nu}{r^2} \frac{\partial u_r}{\partial \theta} = 0, \quad (10)$$

where ν is the kinematic viscosity. Note that here the strongly radial flow assumption is applied so that it holds $u_\theta = 0$. Then the scaling parameters are defined as

$$f(\eta) = r \frac{u_r}{u_c}, \quad \eta = \frac{\theta}{\beta}. \quad (11)$$

By means of these transformations, the continuity equation (8) is automatically satisfied, and the set of momentum equations (9) and (10) is reduced to

$$f''' + 2\beta Re f f' + (4 - Ha)\beta^2 f' = 0, \quad (12)$$

subject to the boundary conditions

$$f(0) = 1, \quad f'(0) = 0, \quad f(1) = C_w, \quad (13)$$

where the prime denotes the derivative to η , C_w , Re and Ha are the stretching or shrinking parameter, the Reynolds number and the Hartmann number, which are defined by

$$C_w = \frac{S_r}{u_c}, \quad Re = \frac{\beta u_c}{\nu}, \quad Ha = \frac{\sigma B_0^2}{\rho \nu}. \quad (14)$$

Note that $C_w > 0$ and $C_w < 0$ respectively represent the stretching and shrinking wall cases.

Physically important quantity for this problem is the local skin friction coefficient, defined by

$$C_{fr} = \frac{\tau_w}{\rho u_c^2}, \quad (15)$$

where τ_w is the wall shear stress, governed by

$$\tau_w = \mu \left(\frac{1}{r} \frac{\partial u}{\partial \theta} \right) \Big|_{\theta=\beta}. \quad (16)$$

Substituting Eq.(16) into Eq.(17), with considering the scaling transformation (11), we obtain

$$C_{fr} = \frac{1}{r^2 Re} f'(1). \quad (17)$$

It is clear that $f'(1)$ is the core part of the local skin friction.

3 Fundamentals of Coiflet wavelet-homotopy method

3.1 Generalized Coiflets wavelet expression

Here the Coiflet wavelet modification technique suggested by Yu *et al.* [27] is employed to solve Eq.(12).

By this approach, the function $g(x)$ ($x \in [0, 1]$) is expressed, for a prescribed resolution level j , by

$$g(x) = \sum_{k=0}^{2^j} g(x_k) \varphi_k(x) + \sum_{s=0}^3 [\alpha_{0,s} \varpi_{0,s}(x) + \alpha_{1,s} \varpi_{1,s}(x)], \quad (18)$$

where k denotes the k th interpolation point, and $g(x_k)$ is the value of $g(x)$ at x_k . $\alpha_{0,s}$ and $\alpha_{1,s}$, $\varpi_{0,s}(x)$ and $\varpi_{1,s}(x)$ are coefficients associated with non-homogenous boundary conditions. For known boundary conditions at certain derivative orders a and/or b ($0 < a < b \leq 3$), it holds

$$\alpha_{0,s} = \begin{cases} g^{(a)}(0), & s = a, \\ g^{(b)}(0), & s = b, \\ 0, & s \neq a \text{ and } s \neq b, \end{cases} \quad \alpha_{1,s} = \begin{cases} g^{(a)}(1), & s = a, \\ g^{(b)}(1), & s = b, \\ 0, & s \neq a \text{ and } s \neq b, \end{cases} \quad (19)$$

and

$$\varpi_{0,s}(x) = \frac{1}{s!} \sum_{i=2-3N+M_1}^{-1} x_i^s \phi_i(x), \quad \varpi_{1,s}(x) = \frac{1}{s!} \sum_{i=2^j+1}^{2^j-1+M_1} (x_i - 1)^s \phi_i(x),$$

where

$$g^{(a)}(0) = \left. \frac{d^a g(x)}{dx^a} \right|_{x \rightarrow 0}, \quad g^{(a)}(1) = \left. \frac{d^a g(x)}{dx^a} \right|_{x \rightarrow 1}.$$

$\varphi_k(x)$ is the generalized weight function, defined by

$$\varphi_k(x) = \begin{cases} \phi_k(x) + \sum_{i=2-3N+M_1}^{-1} T_{0,k}(x_i) \phi_i(x), & k \in [0, 3] \\ \phi_k(x), & k \in [4, 2^j - 4] \\ \phi_k(x) + \sum_{i=2^j+1}^{2^j-1+M_1} T_{1,2^j-k}(x_i) \phi_i(x), & k \in [2^j - 3, 2^j] \end{cases} \quad (20)$$

in which

$$x_i = \frac{i}{2^j}, \quad \phi_i(x) = \phi(2^j x - i + M_1),$$

$$T_{0,k}(x_i) = \sum_{s=0}^3 \frac{p_{0,s,k}}{s!} x_i^s, \quad T_{1,k}(x_i) = \sum_{s=0}^3 \frac{p_{1,s,k}}{s!} (x_i - 1)^s,$$

with $p_{0,s,k}$ and $p_{1,s,k}$ being the matrix elements of the following two matrixes

$$\mathbf{P}_0 = \begin{pmatrix} 1 & 0 & 0 & 0 \\ -11/6 & 3 & -3/2 & 1/3 \\ 2 & -5 & 4 & -1 \\ -1 & 3 & -3 & 1 \end{pmatrix}, \quad \mathbf{P}_1 = \begin{pmatrix} 1 & 0 & 0 & 0 \\ 11/6 & -3 & 3/2 & -1/3 \\ 2 & -5 & 4 & -1 \\ 1 & -3 & -3 & -1 \end{pmatrix}.$$

Here the relations $\mathbf{P}_0 = 2^{i,j} p_{0,s,k}$ and $\mathbf{P}_1 = 2^{i,j} p_{1,s,k}$ are held for $s = 0, 1, 2, 3$.

From the definition of $g(x)$, it is known that its derivatives are only dependent on the weight function $\phi_k(x)$. Therefore we are able to proceed the n th-order derivatives of $g(x)$ by directly differentiating the weight function $\phi_k(x)$ n times with respect to x .

3.2 Linearization

In the framework of the homotopy analysis method, the solution of Eq.(12) can be decomposed into

$$f(\eta) = f_0(\eta) + \sum_{m=1}^M f_m(\eta). \quad (21)$$

The m th-order deformation equation is constructed, for $m \geq 1$, as

$$\mathcal{L}[f_m(\eta) - \chi_m f_{m-1}(\eta)] = c_0 R_m(\eta), \quad (22)$$

subject to the boundary conditions

$$\begin{cases} f_0(0) = 1, & f'_0(0) = 0, & f_0(1) = C_w, & m = 0, \\ f_m(0) = 0, & f'_m(0) = 0, & f_m(1) = 0, & m \geq 1, \end{cases} \quad (23)$$

where c_0 is a homotopy convergence-control parameter, \mathcal{L} is the linear operator, chosen as

$$\mathcal{L} = \frac{\partial^3}{\partial \eta^3},$$

$R_m(\eta)$ is the residual term, defined by

$$R_m(\eta) = f_{m-1}''' + 2\beta R_e \sum_{i=0}^{m-1} f_i f'_{k-1-i} + (4 - H_a)\beta^2 f'_{m-1}, \quad (24)$$

and

$$\chi_m = \begin{cases} 0, & m = 1, \\ 1, & m > 1. \end{cases}$$

The Coiflet wavelet projections are expressed by

$$f_0(\eta) \approx P^j f_0(\eta) = \sum_{k=1}^{2^j-1} f_0(\eta_k) h_k(\eta) + v_0 \varpi_{0,1} + v_1 \varpi_{1,1}, \quad (25)$$

$$f_m(\eta) \approx P^j f_m(\eta) = \sum_{k=1}^{2^j-1} f_m(\eta_k) h_k(\eta), \quad (26)$$

$$R_m(\eta) \approx P^j R_m(\eta) = \sum_{k=0}^{2^j} R_m(\eta_k) \varphi_k(\eta), \quad (27)$$

where P^j denotes the Coiflet wavelet projection, $h_k(\eta)$ is the weight function defined by

$$h_k(\eta) = \varphi(\eta)|_{p_{0,1,k} \rightarrow 0}. \quad (28)$$

The m th-order deformation equation is then expressed via the Coiflet wavelet as

$$\sum_{k=1}^{2^j-1} [f_m(\eta_k) - \chi_m f_{m-1}(\eta_k)] \mathcal{L}[\varphi_k(\eta)] = c_0 \sum_{k=0}^{2^j} R_m(\eta_k) \varphi_k(\eta). \quad (29)$$

Eq.(29) is solved by means of the Galerkin method. Multiplying both sides of Eq.(29) by $h_k(\eta)$ and integrating in the domain $[0,1]$, we obtain

$$\mathbf{A}^T (\hat{f}_m - \chi_m \hat{f}_{m-1}) = c_0 \mathbf{B}^T \hat{R}_m, \quad (30)$$

where

$$\hat{f}_m = [f_m(\eta_1), f_m(\eta_2), \dots, f_m(\eta_{2^j-1})]^T,$$

$$\hat{R}_m = [R_m(0), R_m(\eta_1), \dots, R_m(1)]^T,$$

and

$$\mathbf{A} = \begin{bmatrix} a_{1,1} & a_{1,2} & \cdots & a_{1,2^j-1} \\ a_{2,1} & a_{2,2} & \cdots & a_{2,2^j-1} \\ \vdots & \vdots & \vdots & \vdots \\ a_{2^j-1,1} & a_{2^j-1,2} & \cdots & a_{2^j-1,2^j-1} \end{bmatrix}$$

and

$$\mathbf{B} = \begin{bmatrix} b_{0,1} & b_{0,2} & \cdots & b_{0,2^j-1} \\ b_{1,1} & b_{1,2} & \cdots & b_{1,2^j-1} \\ \vdots & \vdots & \vdots & \vdots \\ b_{2^j,1} & b_{2^j,2} & \cdots & b_{2^j,2^j-1} \end{bmatrix}$$

in which, $a_{k,l}$ and $b_{k,l}$ are defined as

$$a_{k,l} = \Gamma_{k,l,3}, \quad b_{k,l} = \bar{\Gamma}_{k,l,0}. \quad (31)$$

with the connection coefficients being given by

$$\Gamma_{k,l,n} = \int_0^1 \frac{d^n h_k(\eta)}{d\eta^n} h_l(\eta) d\eta, \quad \bar{\Gamma}_{k,l,n} = \int_0^1 \frac{d^n \phi_k(\eta)}{d\eta^n} h_l(\eta) d\eta, \quad (32)$$

3.3 Validation

To ensure the accuracy of our proposed approach, the quadratic Riccati differential equation [30] is used as an illustrative example, which is written as

$$Y'(t) - 2Y + Y^2 - 1 = 0, \quad (33)$$

subject to the initial conditions

$$Y(0) = 0. \quad (34)$$

The above nonlinear system admits the exact solution

$$Y(t) = 1 + \sqrt{2} \tanh \left[\sqrt{2}t + \frac{1}{2} \ln \left(\frac{\sqrt{2} - 1}{\sqrt{2} + 1} \right) \right]. \quad (35)$$

In the framework of the homotopy analysis method, the initial guess and the linear operator are chosen as

$$Y_0(t) = 0, \quad \mathcal{L} = \frac{d}{dt}. \quad (36)$$

By means of our above-mentioned approach, under the definitions

$$\begin{cases} a_{l,k} = \Gamma_{k,l,1} \\ b_{l,k} = \Gamma_{k,l,0}, \end{cases} \quad (37)$$

we are able to obtain the following M th-order wavelet solution

$$\tilde{Y}_M(t) = Y_0(t) + \sum_{m=1}^M Y_m(t). \quad (38)$$

To check its accuracy and efficiency, the averaged square error $Err_{s,M}$ and the relative error $Err_{r,M}$ are introduced, which are written by

$$Err_{s,M} = \frac{1}{(2^j + 1)} \sum_{k=0}^{2^j} \left[\tilde{Y}_M(t_k) - \tilde{Y}_E(t_k) \right]^2, \quad (39)$$

$$Err_{r,M} = \frac{|\tilde{Y}_M(t) - \tilde{Y}_E(t)|}{|\tilde{Y}_E(t)|}, \quad (40)$$

where $t_k = k/2^j$, \tilde{Y}_M and \tilde{Y}_E represent the M th-order wavelet approximation and the exact solution respectively.

Table 1 presents the averaged square error at different computational order M and resolution level j . All results are obtained by using the same desktop computer, with its configuration being the processor Intel(R) Core(TM) i3-5015U CPU @ 2.10GHz, and installed memory(RAM) 4.00GB. It is seen from the table that both the computational order M and the resolution level j play key roles on error reduction. Further to check the accuracy of the Coiflet wavelet-homotopy solutions, we compare the 120th-order

Table 1: The averaged square error given by Eq.(39) at $c_0 = -0.08$.

	j=3	j=4	j=5
50th order	1.52×10^{-3}	1.20×10^{-3}	1.06×10^{-3}
CPU time (second)	0.25	0.27	0.39
80th order	4.26×10^{-5}	4.617×10^{-5}	4.31×10^{-5}
CPU time (second)	0.29	0.32	0.43
100th order	1.90×10^{-5}	5.89×10^{-5}	4.44×10^{-6}
CPU time (second)	0.28	0.28	0.43
120th order	3.29×10^{-5}	7.4328×10^{-6}	7.43×10^{-6}
CPU time (second)	0.30	0.30	0.52

solution at the resolution levels $j = 3$, $j = 4$ and $j = 5$ with the exact solution (35), very excellent agreement is found, as shown in Table 2. This confirms the validity of our proposed method.

4 Results

In this section, the accuracy of our Coiflet solution is verified. The check procedure is divided into two steps. We first examine the residual error of the solution itself. It has known that Eq.(12) does not admit an analytical solution, we therefore introduce the relative error as its convergent indicator. In doing so, we define

$$ResErr_m = \frac{1}{(2^j + 1)} \sum_{k=0}^{2^j} [f_{M+1}(\eta_k) - f_M(\eta_k)]^2, \quad (41)$$

where $f_M(\eta_k)$ and $f_{M+1}(\eta_k)$ are the M th-order and the $(M+1)$ th-order Coiflet wavelet-homotopy solutions.

For the sake of simplicity, we consider the particular case $C_w = 0$. Other mathematical and physical

Table 2: Comparison of the exact solution with Coiflet-homotopy ones for different resolution levels j at $c_0 = 0.08$.

t	Exact Solution	Our solution		
		$j = 3$	$j = 4$	$j = 5$
0	0	0	0	0
1/8	0.141185	0.140195	0.140904	0.141183
2/8	0.315927	0.315038	0.315353	0.315915
3/8	0.522987	0.522206	0.522891	0.522982
4/8	0.756016	0.755570	0.755918	0.756013
5/8	1.003541	1.002603	1.003508	1.003530
6/8	1.250860	1.250055	1.250845	1.250859
7/8	1.483291	1.483207	1.483274	1.483280
1	1.689499	1.689401	1.689438	1.689497

parameters are chosen as $c_0 = 0.1$, $Ha = 1000$, $Re = 50$ and $\beta = 5$, respectively. As shown in Fig.2, the relative residual error decreases rapidly as the computational order evolves for all considered resolution levels. The maximum relative error is less than 1×10^{-7} at 120th order computation.

We then compare our results with the published ones in literature. It is seen from Table 3 and Table 4 that our solution matches the published ones for both convergent and divergent channels. This further confirms the validity and accuracy of our proposed approach. Note that here the range of c_0 is chosen

from the range $[-0.5, -0.08]$ and $Ha = 0$.

Table 3: Comparison of $f''(0)$ by our proposed approach with the published ones for different values of Re at $\beta = -5$.

	$Re = 10$	$Re = 30$	$Re = 50$	$Re = 70$	$Re = 100$
Mosta <i>et al.</i> [6]	-1.784547	-1.413692	-1.121989	-0.893474	-0.640178
Turkyilmazoglu [32]	-1.784546	-1.413691	-1.121989	-0.893474	-0.640177
Our results	-1.784547	-1.413691	-1.121989	-0.893473	-0.640177

Table 4: Comparison of $f''(0)$ by our proposed approach with the published ones for different values of Re at $\beta = 5$.

	$Re = 20$	$Re = 60$	$Re = 100$	$Re = 140$	$Re = 180$
Mosta <i>et al.</i> [6]	-2.527192	-3.942140	-5.869165	-8.207326	-10.792073
Turkyilmazoglu [32]	-2.527192	-3.942140	-5.869165	-8.207326	-10.792073
Our results	-2.527191	-3.942140	-5.869164	-8.207325	-10.792072

In addition, we discuss the efficiency of our proposed technique. It has known that the traditional Coiflet wavelet approach [22] is equivalent to the first order Coiflet wavelet-homotopy computation at $c_0 = -1$. As a result we only need to compare our proposed method with the traditional optimized homotopy analysis method. The comparison is listed in Table 5 and Table 6, in which we find that our

proposed approach is more than 100 times faster than the traditional homotopy analysis method when the values of $f'(1)$ obtained by both techniques are same for four decimal places. Note that in these cases the convergence control parameter is chosen from the range $[-0.5, -0.2]$ for both approaches.

Table 5: CPU time comparison of the optimized homotopy analysis method (HAM) and the Coiflet wavelet-homotopy method (CWHAM) for different values of Ha at $Re = 50$ and $\beta = -5$.

Ha	$C_w = 2$			$C_w = -2$		
	$f'(1)$	HAM	CWHAM	$f'(1)$	HAM	CWHAM
100	3.7593	162.45	1.20	-5.3650	180.18	0.92
500	4.1046	177.03	1.18	-6.2586	182.40	0.88
1000	4.8148	175.29	0.98	-9.0548	176.61	0.88
2000	5.2469	174.09	0.93	-12.0284	213.09	0.87
5000	3.7372	109.46	0.93	-18.5583	143.86	0.91
		second	second		second	second

Mathematically, it is always a challenge work to give accurate solutions to nonlinear equations with physical parameters being chosen from a extremely wide region. Here we test the capability of our proposed technique for handling such problems, while the optimized homotopy analysis method and the standard shooting technique are employed as the contrasts. A large range of the Hartmann numbers are computed for examining the adaptability of our proposed technique. As shown in Table 7 and Table 8. For small and medium Ha , all computational approaches give very excellent results. As Ha

Table 6: CPU time comparison of the optimized homotopy analysis method (HAM) and the Coiflet wavelet-homotopy method (CWHAM) for different values of Ha at $Re = 50$ and $\beta = 5$.

Ha	$C_w = 2$			$C_w = -2$		
	$f'(1)$	HAM	CWHAM	$f'(1)$	HAM	CWHAM
100	-0.7862	192.285	0.89	-7.1847	241.59	0.85
500	0.1808	185.216	0.93	-8.3887	187.58	0.83
1000	1.1088	181.862	0.82	-9.8086	191.49	0.80
2000	2.4989	179.982	0.85	-12.3920	185.24	0.85
5000	5.1925	111.448	0.84	-18.5887	175.90	0.84
		second	second		second	second

continuously increases, the optimized homotopy analysis method and the standard shooting technique gradually fail to give accurate solutions, while our proposed method still keeps accurate. Note that the integration distance by shooting technique is designated as $\eta_{max} = 20, 30, 40$ respectively, the step size is $\Delta\eta = 0.005, 0.01, 0.05$ correspondingly. Only all results for a prescribed set of physical parameters with varying integration distances and step sizes remain same, they are deemed as stable. The Newtonian iteration is executed with the convergent criteria of 1.0×10^{-8} for all considered cases.

The physical aspects of the problem are discussed in the following part. The flow velocity behaviors under the influence of different physical parameters are portrayed Fig.3-Fig.8. In Fig.3 and Fig.4, the effects of the stretching/shrinking parameter C_w on the flow velocity $f(\eta)$ driven in convergent channel

Table 7: Comparison of $f'(1)$ by the optimized homotopy analysis method (HAM), the shooting method (SHOOTM), and the Coiflet wavelet-homotopy method (CWHAM) for different values of Ha at $Re = 50$ and $\beta = -5$.

Ha	$C_w = 1.5$			$C_w = -1.5$		
	HAM	SHOOTM	CWHAM	HAM	SHOOTM	CWHAM
100	1.76212	1.76212	1.76213	-5.43485	-5.43485	-5.43484
500	1.96503	1.96503	1.96502	-6.70401	-6.70401	-6.70400
1000	2.17478	2.17478	2.17477	-8.09765	-8.09764	-8.09766
10000	4.64589	4.64579	4.64589	-3.04261	-3.04262	-3.04261
100000	—	—	3.19212	—	-	-2.53802
1000000	—	—	2.07773	—	-	-2.53548

($\beta = -5$) and divergent channel ($\beta = 5$) for the fixed values $Ha = 50$ and $Re = 50$ are presented. Clearly the case $C_w = 0$ represents flow driven through a channel with stationary walls, which has been discussed by Esmailpour *et al.* [7]. And the case $C_w = 1$ physically indicates that the stretching velocity of the channel wall is identical to the flow velocity. For the case $C_w > 1$, the velocity of fluid increases faster than the centreline velocity u_c . It means that the fluid particles intensifies very close to the channel wall owing to the influence of the viscosity and inertia of the fluid, just like the polymers concentrate close to the convergent channel rather than the centreline of the channel. For the case $C_w < 0$, the wall stretching direction is opposite to the fluid flow direction, the flow is retarded owing to the resistance of the reverse force generated by the shrinking walls. It is found that in both cases the velocity profiles

Table 8: Comparison of $f'(1)$ by the optimized homotopy analysis method (HAM), the shooting method (SHOOTM), and the Coiflet wavelet-homotopy method (CWHAM) for different values of Ha at $Re = 50$ and $\beta = 5$.

Ha	$C_w = 1.5$			$C_w = -1.5$		
	HAM	SHOOTM	CWHAM	HAM	SHOOTM	CWHAM
100	12.51506	12.51506	12.51505	-5.35377	-5.35377	-5.35375
500	12.83738	12.83737	12.83738	-6.41662	-6.41662	-6.41661
1000	0.74015	0.74014	0.74014	-7.65832	-7.65831	-7.65832
10000	4.62507	4.62507	4.62506	-21.61287	-21.61287	-21.61286
100000	—	—	3.10626	—	—	-1.53998
1000000	—	—	5.00934	—	—	-0.29484

increase as C_w enlarges. In addition, the effects of stretching/shrinking wall parameters on the wall skin friction (wall shear stress) for both convergent and divergent channels are tabulated in the Table 9 and Table 10. It is seen that the results by the Coiflet wavelet-homotopy method (CWHAM) matches those by the optimized homotopy analysis method (HAM) and the shooting method (SHOOTM) in the whole domain. On the other hand, we notice that the increase in C_w leads to the increase in the skin friction $f'(1)$ for both convergent and divergent cases. For the shrinking wall case, the shear forces by the channel wall and by the fluid motion have same directions. While for the stretching wall case, they have opposite direction.

Table 9: Influence of the stretching/shrinking parameter on the skin friction coefficient $f'(1)$ for the convergent channel ($\beta = -5$) at $Ha = 50$ and $Re = 50$.

C_w	CWHAM	HAM	SHOOTM
-1.5	-5.263467	-5.263465	-5.263467
-1	-4.712285	-4.712286	-4.712285
-0.8	-4.173127	-4.173127	-4.173128
-0.5	-3.973255	-3.973254	-3.973254
0	-2.888555	-2.888552	-2.888553
0.5	-1.843952	-1.843953	-1.843952
1.0	0.000000	0.000000	0.000000
1.5	2.254527	2.254526	2.254527
2.0	3.714635	3.714636	3.714635

The effects of the Reynolds number Re on the velocity profile $f(\eta)$ for convergent and divergent channels are depicted Fig.5 and Fig.6 respectively. It is clearly observed that the increase in Reynolds number Re leads to the increase in the velocity profile $f(\eta)$ for the shrinking and convergent channel case, while results in the decrease in the velocity profile $f(\eta)$ for stretching of convergent channel. However the totally opposite behaviors are observed for the divergent channel case. The variation of velocity profile $f(\eta)$ under the action of the Hartmann number for the convergent channel case is illustrated in Fig.7. It is noticed from the figure that, an augmentation of Hartmann number Ha , the velocity profile $f(\eta)$ decreases for the stretching wall case and opposite behaviors shows for the shrinking wall case.

Table 10: Influence of the stretching/shrinking parameter on the skin friction coefficient $f'(1)$ for the divergent channel ($\beta = 5$) at $Ha = 50$ and $Re = 50$.

C_w	CWHAM	HAM	SHOOTM
-1.5	-5.220584	-5.220584	-5.220585
-1	-3.785589	-3.785587	-3.785589
-0.5	-2.268185	-2.268186	-2.268185
-0.2	-1.902586	-1.902586	-1.902586
0	-1.178779	-1.178780	-1.178782
0.5	-0.582525	-0.582524	-0.582525
1.0	0.000000	0.000000	0.000000
1.3	1.291167	1.291167	1.291168
1.5	1.473324	1.473324	1.473325

This is due to the change in Hartmann number Ha leads to the variation of the Lorentz force. Consequently, the modified Lorentz force is responsible for an elevated resistance of flow transfer in the case of stretching and shrinking of the channel. Fig.8 demonstrates the effect of Hartmann number Ha on velocity profile $f(\eta)$ for divergent wall case. Similar variational trend is observed owing to the Lorentz force exerts equivalent influence as aforementioned case. Note that all the results illustrated in Fig.3-Fig.8 are obtained with the the convergent control parameter being chosen in the range $[-0.008, -0.5]$.

5 Conclusions

We have established the new numerical algorithm for the nonlinear MHD Jeffery Hamel problem based on the Coiflet wavelet-homotopy method. The proposed method has been checked rigidly. Results reveal that the newly developed technique is superior to the optimized homotopy analysis method, which is capable of handling strong nonlinear problems with higher efficiency. Especially, it can give accurate solutions for extreme wide ranges of physical parameters. Besides, the physical mechanism of the flow problem has been presented and discussed. Some major physical findings of the current work are as follows:

- For both convergent and divergent channel cases, wall stretching drags more fluid from the channel wall, while wall shrinking pulls the fluid to the wall and causes the back flow.
- The wall stretching of a divergent channel gives similar flow pattern as the wall shrinking of a convergent channel, or vice-versa.
- The Hartmann number Ha plays a key role on the flow velocity distribution. While opposite trends are obtained for stretching convergent channel case and shrinking divergent channel case.

Acknowledgment

This work is partially supported by the National Natural Science Foundation of China (Grant No. 11872241).

Author contributions

S. Ahmed performed the mathematical modeling and prepared figures and table form. H.Xu wrote the whole manuscript text. A.Y. Wang and Q.B. Chen examined the formulation of the Coiflet wavelet. All authors reviewed the manuscript.

Competing interests

The authors declare no competing interests.

Additional information

Correspondence and requests for materials should be addressed to H. Xu.

References

- [1] Jeffery, G.B. The two-dimensional steady motion of a viscous fluid. *London, Edinburgh, Dublin Philos. Mag. J. Sci.* **29**, 455–465. <https://doi.org/10.1080/14786440408635327> (1915).
- [2] Hamel, G. Spiralförmige Bewegungen Zäher Flüssigkeiten. *Jahresber. Dtsch. Math. Ver.* **25**, 34–60. (1917).
- [3] Rosenhead, L. The steady two-dimensional radial flow of viscous fluid between two inclined plane walls. *Proc. R. Soc. A-Math. Phys. Eng. Sci.* **175**, 436–467. <https://doi.org/10.1098/rspa.1940.0068> (1940).

- [4] Fraenkel, L.E. Laminar flow in symmetrical channels with slightly curved walls. II. An asymptotic series for the stream function. *Proc. R. Soc. A-Math. Phys. Eng. Sci.* **272**, 406–428. <https://doi.org/10.1098/rspa.1963.0061> (1963).
- [5] Axford, W.I. The magnetohydrodynamic Jeffery-Hamel problem for a weakly conducting fluid. *Q. J. Mech. Appl. Mech.* **14**, 335–351. <https://doi.org/10.1093/qjmam/14.3.335> (1961).
- [6] Motsa, S.S., Sibanda, P., Awad, F.G., & Shateyi, S. A new spectral-homotopy analysis method for the MHD Jeffery-Hamel problem. *Comput. Fluids* **39**, 1219–1225. <https://doi.org/10.1016/j.compfluid.2010.03.004> (2010).
- [7] Esmaeilpour, M. & Ganji, D.D. Solution of the Jeffery-Hamel flow problem by optimal homotopy asymptotic method. *Comput. Math. Appl.* **59**, 3405–3411. <https://doi.org/10.1016/j.camwa.2010.03.024> (2010).
- [8] Esmaili, Q., Ramiar, A., Alizadeh, E. & Ganji, D.D. An approximation of the analytical solution of the Jeffery-Hamel flow by decomposition method. *Phys. Lett. A* **372**, 3434–3439. <https://doi.org/10.1016/j.physleta.2008.02.006> (2008).
- [9] Sheikholeslami, M., Ganji, D.D., Ashorynejad, H.R. & Rokni, H.B. Analytical investigation of Jeffery-Hamel flow with high magnetic field and nanoparticle by Adomian decomposition method. *Appl. Math. Mech.-Engl. Ed.* **33**, 25–36. <https://doi.org/10.1007/s10483-012-1531-7> (2012).
- [10] Dib, A., Haiahem, A. & Bou-said, B. An analytical solution of the MHD Jeffery-Hamel flow by the modified Adomian decomposition method. *Comput. Fluids* **102**, 111–115. <https://doi.org/10.1016/j.compfluid.2014.06.026> (2014).

- [11] Makinde, O.D. Effect of arbitrary magnetic Reynolds number on MHD flows in convergent-divergent channels. *Int. J. Numer. Methods Heat Fluid Flow*, **18**, 697–707. <https://doi.org/10.1108/09615530810885524> (2008).
- [12] Domairry, G., Mohsenzadeh, A. & Famouri, M. The application of Homotopy analysis method to solve nonlinear differential equation governing Jeffery-Hamel flow. *Commun. Nonlinear Sci. Numer. Simul.* **14**, 85–95. <https://doi.org/10.1016/j.cnsns.2007.07.009> (2008).
- [13] Ganji, Z.Z., Ganji, D.D. & Esmailpour, M. Study on nonlinear Jeffery-Hamel flow by He's semi-analytical methods and comparison with numerical results. *Comput. Math. Appl.* **58**, 2107–2116. <https://doi.org/10.1016/j.camwa.2009.03.044> (2009).
- [14] Ahmad, I. & Ilyas, H. Homotopy perturbation method for the nonlinear MHD Jeffery-Hamel blood flows problem. *Appl. Numer. Math.* **141**, 124–132. <https://doi.org/10.1016/j.apnum.2018.07.005> (2019).
- [15] Rana, P., Shukla, N., Gupta, Y., & Pop, I. Analytical prediction of multiple solutions for MHD Jeffery-Hamel flow and heat transfer utilizing KKL nanofluid model. *Phys. Lett. A* **383**, 176–185. <https://doi.org/10.1016/j.physleta.2018.10.026> (2019).
- [16] Anitha, S., Thomas, T., Parthiban, V. & Pichumani, M. What dominates heat transfer performance of hybrid nanofluid in single pass shell and tube heat exchanger? *Adv. Powder Technol.* **30**, 3107–3117. <https://doi.org/10.1016/j.appt.2019.09.018> (2019).
- [17] Onyango, E.R., Kinyanjui, M.N.K., Kimathi, M. & Uppal, S.M. Heat and mass transfer on MHD Jeffrey-Hamel flow in presence of inclined magnetic field. *Appl. Comput. Math.* **9**, 108–117. <https://doi.org/10.11648/j.acm.20200904.11> (2020).

- [18] Liao, S.J. *The proposed homotopy analysis technique for the solution of nonlinear problems*. Ph.D thesis, Shanghai Jiao Tong University, China, 1992.
- [19] Liao, S.J. *Beyond perturbation: Introduction to the homotopy analysis method*. Chapman & Hall /CRC Press, Boca Raton, 2003.
- [20] Yang, Z.C. & Liao, S.J. A HAM-based wavelet approach for nonlinear ordinary differential equations. *Commun. Nonlinear Sci. Numer. Simul.* **48**, 439–453. <https://doi.org/10.1016/j.cnsns.2017.01.005> (2017).
- [21] Yang, Z.C. & Liao, S.J. A HAM-based wavelet approach for nonlinear partial differential equations: Two dimensional Bratu problem as an application. *Commun. Nonlinear Sci. Numer. Simul.*, **53**, 249–262. <https://doi.org/10.1016/j.cnsns.2017.05.005> (2017).
- [22] Wang, J.Z. *Generalized theory and arithmetic of orthogonal wavelets and applications to researches of mechanics including piezoelectric smart structures*. Ph.D thesis, Lanzhou University, China, 2001.
- [23] Liu, X.J., Zhou, Y.H., Wang, X. & Wang, J.Z. A wavelet method for solving a class of nonlinear boundary value problems. *Commun. Nonlinear Sci. Numer. Simul.*, **18**, 1939–1948. <https://doi.org/10.1016/j.cnsns.2012.12.010> (2013).
- [24] Zhou, Y.H. & Wang, J.Z. Generalized Gaussian integral method for the calculation of scaling function transforms of wavelets and its applications. *Acta Math. Sci. A*, **19**, 293–300. <https://doi.org/10.3321/j.issn:1003-3998.1999.03.008> (1999).

- [25] Yu, Q. & Xu, H. Novel wavelet-homotopy Galerkin technique for analysis of lid-driven cavity flow and heat transfer with non-uniform boundary conditions. *Appl. Math. Mech.-Engl. Ed.* **39**, 1691–1718. <https://doi.org/10.1007/s10483-018-2397-9> (2018).
- [26] Yu, Q., Xu, H. & Liao, S.J. Analysis of mixed convection flow in an inclined lid-driven enclosure with Buongiorno's nanofluid model. *Int. J. Heat Mass Transf.* **126**, 221–236. <https://doi.org/10.1016/j.ijheatmasstransfer.2018.05.109> (2018).
- [27] Yu, Q., Xu, H., & Liao, S.J. Nonlinear analysis for extreme large bending deflection of a rectangular plate on non-uniform elastic foundations. *Appl. Math. Model.* **61**, 316–340. <https://doi.org/10.1016/j.apm.2018.04.022> (2018).
- [28] Wang, A.Y., Xu, H. & Yu, Q. Homotopy Coiflets wavelet solution of electrohydrodynamic flows in a circular cylindrical conduit. *Appl. Math. Mech.-Engl. Ed.* **41**, 681–698. <https://doi.org/10.1007/s10483-020-2607-8> (2020).
- [29] Chen, Q.B. & Xu, H. Coiflet Wavelet-Homotopy solution of channel flow due to orthogonally moving porous walls governed by the Navier-Stokes equations. *J. Math.* **2020**, Article ID 5739648, 12 pages. <https://doi.org/10.1155/2020/5739648> (2020).
- [30] Tana, Y. & Abbasbandy, S. Homotopy analysis method for quadratic Riccati differential equation. *Commun. Nonlinear Sci. Numer. Simul.* **13**, 539-546. <https://doi.org/10.1016/j.cnsns.2006.06.006> (2008).
- [31] Xu, H. & Liao, S.J. Series solutions of unsteady MHD flows above a rotating disk. *Meccanica* **41**, 599–609. <https://doi.org/10.1007/s11012-006-9006-x> (2006).

- [32] Turkyilmazoglu, M. Extending the traditional Jeffery-Hamel flow to stretchable convergent/divergent channels. *Comput. Fluids* **100**, 196–203. <https://doi.org/10.1016/j.compfluid.2014.05.016> (2014).

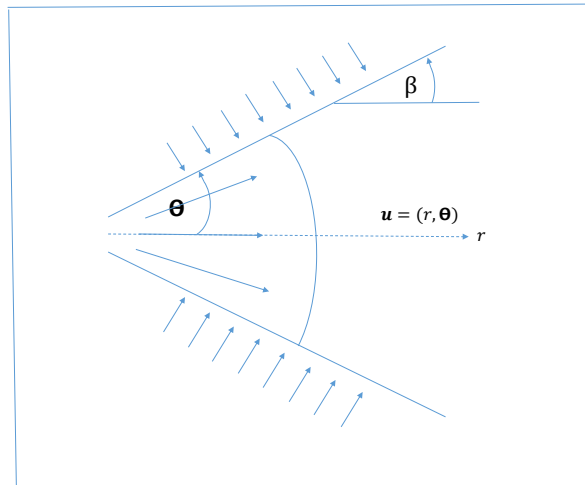


Fig.1: Physical sketch of the magnetised Jeffery-Hamel flow.

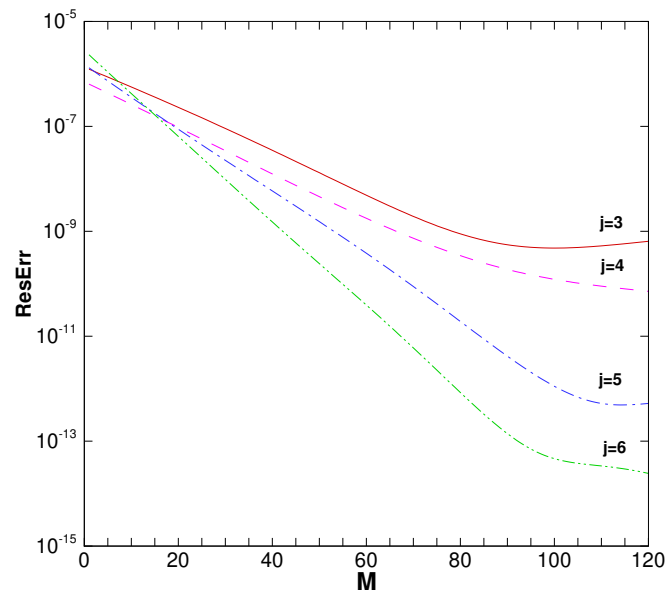


Fig.2: The residual error denoted in versus the computational order M for $\beta = 5$, $Ha = 1000$ with different resolution levels in the case of the convergence-control parameter $c_0 = -0.1$.

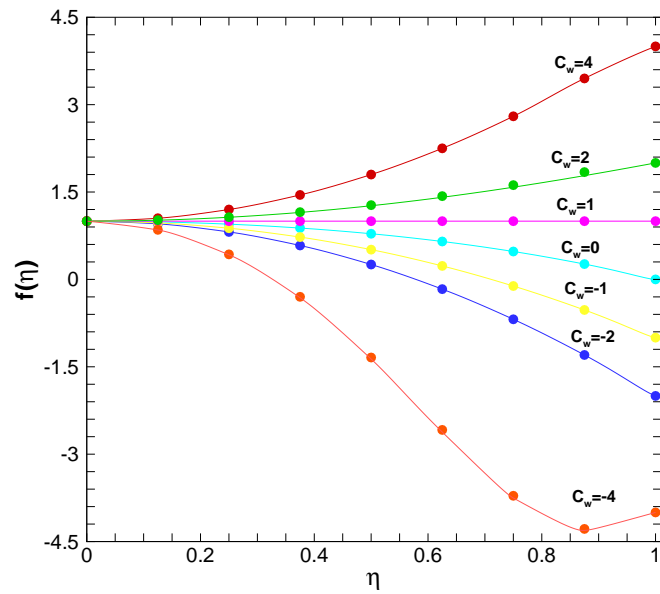


Fig.3: Effects of stretching and shrinking walls on the velocity profile $f(\eta)$ at specific values of $\beta = -5$, $Ha = 50$ and $Re = 50$. Line: Coiflet wavelet solution; Circle: Shooting solution.

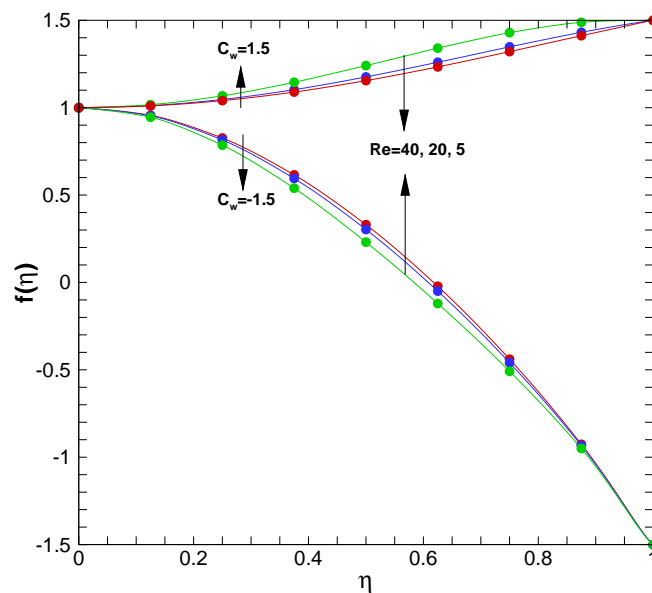


Fig.4: Effects of stretching and shrinking walls on the velocity profile $f(\eta)$ at specific values of $\beta = 5$, $Ha = 50$ and $Re = 50$. Line: Coiflet wavelet solution; Circle: Shooting solution.

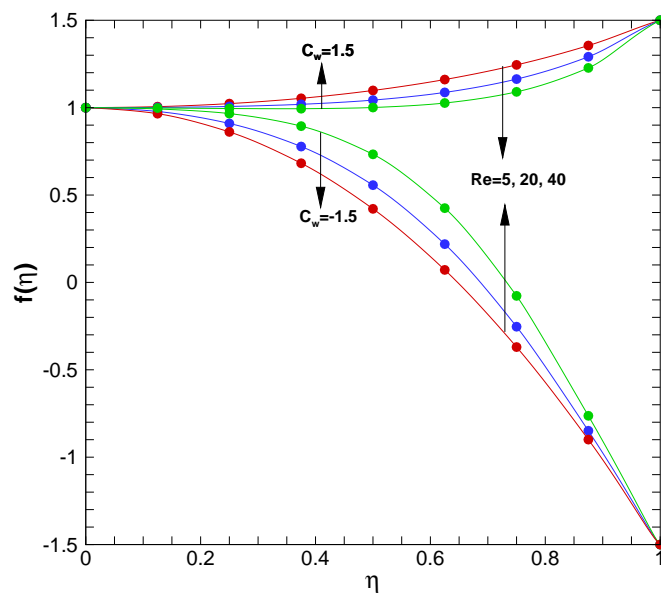


Fig.5: Effects of the Reynolds number Re on the velocity profile $f(\eta)$ at specific values of $\beta = -3$ and $Ha = 5$. Line: Coiflet wavelet solution; Circle: Shooting solution.

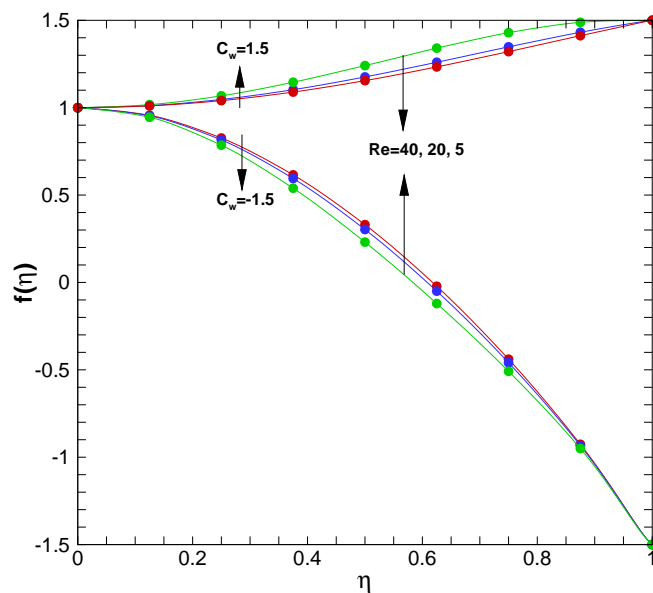


Fig.6: Effects of the Reynolds number Re on the velocity profile $f(\eta)$ at specific values of $\beta = 3$ and $Ha = 5$. Line: Coiflet wavelet solution; Circle: Shooting solution.

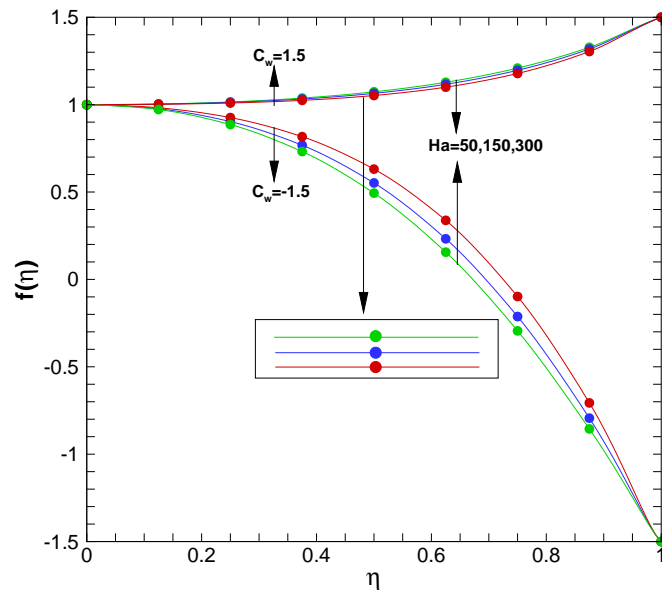


Fig.7: Effects of the Hartmann number Ha on the velocity profile $f(\eta)$ at specific values of $\beta = -3$ and $Re = 10$ Line: Coiflet wavelet solution; Circle: Shooting solution.

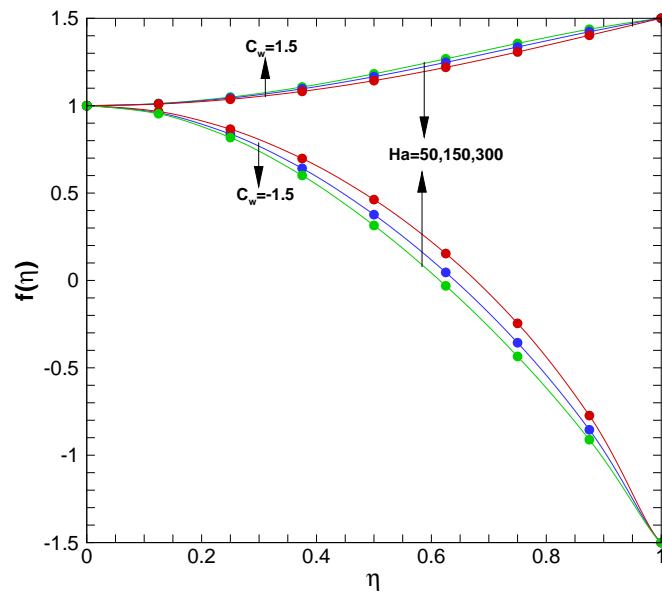


Fig.8: Effects of the Hartmann number Ha on the velocity profile $f(\eta)$ at specific values of $\beta = 3$ and $Re = 10$ Line: Coiflet wavelet solution; Circle: Shooting solution.